Large deformation bending analysis of functionally graded spherical shell using FEM

Vishesh Ranjan Kar[a] and Subrata Kumar Panda[*]

Department of Mechanical Engineering, National Institute of Technology, Rourkela, India

Abstract. In this article, nonlinear finite element solutions of bending responses of functionally graded spherical panels are presented. The material properties of functionally graded material are graded in thickness direction according to a power-law distribution of volume fractions. A general nonlinear mathematical shallow shell model has been developed based on higher order shear deformation theory by taking the geometric nonlinearity in Green-Lagrange sense. The model is discretised using finite element steps and the governing equations are obtained through variational principle. The nonlinear responses are evaluated through a direct iterative method. The model is validated by comparing the responses with the available published literatures. The efficacy of present model has also been established by demonstrating a simulation based nonlinear model developed in ANSYS environment. The effects of power-law indices, support conditions and different geometrical parameters on bending behaviour of functionally graded shells are obtained and discussed in detail.

1. Introduction

In the present scenario, many advanced materials are being developed rapidly and being used in different engineering structures/structural components to make a compromise between the strength and the cost. This in turn creates the necessity of analysis of these materials and structures to meet the design and/or analysis requirement. In this regard, laminated composites have been widely appreciated and dominated by many weight sensitive industries for last few decades. However, these multi-layer composites are incapable of carrying extra amount of load and excessive thermal distortion due to de-lamination phenomenon. De-lamination has been a major problem of concern reported by many researchers in the reliable design of laminated composites. In addition to that, the separation of layers caused by high local inter-laminar stresses result in destruction of load transfer mechanism, reduction of stiffness and loss of structural integrity leading to final structural and functional failure. In order to bridge the gap, recently a new type of material known as functionally graded material (FGM) has been developed by grading the volume fraction of two counterparts, namely, metals and ceramics. It is worthy to mention that, the metals have already

---

∗Corresponding author, Assistant Professor, E-mail: call2subrat@gmail.com
[a]Ph.D. Student, E-mail: visheshkar@gmail.com

established their existence and capabilities in engineering field for many years for their excellent strength and toughness, whereas ceramic materials have shown their capabilities in heat resistance and anti-oxidant properties (Reddy 2003). The gradual variation results in a very efficient material tailored to meet the requirement of current structures operating in very extreme conditions such as aircraft engines, rocket heat shields, heat exchanger tubes, thermal barrier coatings, etc.

Most of the studies of this class of material are limited to a computational analysis because of the complexity and expensiveness in synthesis. The modelling and analysis of functionally graded (FG) structures has been continued from last two decades to come up with the new/modified mathematical model and solution techniques to overcome the drawbacks of the former studies (Birman and Byrd 2007, Liew *et al*. 2011, Jha *et al*. 2013, Alijani and Amabili 2014). Many researchers investigated the linear and nonlinear bending behaviour of FG flat/shell panels incorporating the mid-plane kinematics based on different shear deformation and classical theories.

Woo and Meguid (2001) studied large deflection of FG plates and shallow shells based on classical plate theory (CPT) with von Karman's nonlinear strain terms under mechanical and thermal loading. Shen (2002) presented an analytical solution to nonlinear bending of FG plate based on the HSDT kinematics. Bian *et al*. (2006) investigated bending and free vibration of a simply supported hybrid FG plate with an intermediate piezoelectric layer using elasticity method based on state space formulations. Navazi and Haddadpour (2008) developed an exact solution for nonlinear analysis of shear deformable FG plate using first order shear deformation theory (FSDT) model with the incorporation of the von Karman nonlinear strain terms. Zhao *et al*. (2009) analysed the static response and free vibration FG shell panels for different parameters (volume fraction, material property, support condition and thickness ratio) using the element-free kp-Ritz method. In their model, the displacement field is expressed in terms of asset of mesh-free kernel particle functions according to Sander's first order shear deformation shell theory. Zhao and Liew (2009a, b) investigated the nonlinear response of FG flat and cylindrical panels using the element-free kp-Ritz method based on a modified version of Sander's nonlinear shell theory under mechanical and thermal loads. Santos *et al*. (2009) developed a semi-analytical axisymmetric finite element model using the 3D linear elastic theory to obtain bending and vibration response of FG cylindrical panel. Talha and Singh (2010) investigated free vibration and static behaviour of shear deformable FG plates based on the HSDT with a modification in the transverse displacement function. Mao *et al*. (2011) have investigated contact force and dynamic response of FGM shallow spherical shell under low velocity impact in thermal environment and developed Giannakopoulos's 2-D contact model to predict contact force in analysis of FGM shallow spherical shell under low velocity impact. Bich and Tung (2011) presented an analytical approach to investigate the nonlinear axisymmetric response of FGM shallow spherical shells subjected to uniform external pressure with and without including the effects of temperature conditions. Neves *et al*. (2011, 2012) developed sinusoidal shear deformation model of FG plates and evaluated the bending and vibration responses using collocation method based on the radial basis functions. Oktem *et al*. (2012) presented the static behaviour of simply-supported FG plates and doubly curved shells based on the HSDT model. The authors also developed a new HSDT model and investigated the bending response of FG plate (Mantari *et al*. 2012). Bich *et al*. (2012) investigated nonlinear static and dynamic unsymmetrical responses of FG shallow spherical shells analytically under external pressure incorporating the effects of temperature. Xiang and Kang (2013) implemented an nth -order shear deformation theory and mesh-less global collocation method for bending analysis of a simply supported functionally graded plate under sinusoidal load. Zenkour

and Sobhy (2013) incorporated sinusoidal shear deformation plate theory to obtain thermoelastic bending response of a simply supported FG plate resting on Pasternak's elastic foundation. Thai and Kim (2013) developed a new higher order shear deformation theory (HSDT) model to analyse bending and free vibration behaviour of FG plates. Zhang *et al.* (2014) investigated the thermal and mechanical buckling behavior of FG plates by using local Kriging meshless method. Zhu *et al.* (2014) performed a nonlinear thermo-mechanical analysis of FG flat panels using FSDT mid-plane kinematics and von Karman nonlinearity by adopting a local meshless method and Kriging interpolation technique. Lei *et al.* (2014) investigated the dynamic stability analysis of carbon nanotube-reinforced FG (CNTR-FG) cylindrical shell panels using the mesh-free kp-Ritz method. Liew *et al.* (2014) employed the element-free kp-Ritz method to analyze post-buckling of CNTR-FG cylindrical panels based on the FSDT and the von Karman strain terms. Zhang *et al.* (2014a, b) analysed the linear and the nonlinear flexural responses of CNTRC-FG cylindrical panels using the FSDT kinematics and the mesh-free kp-Ritz method.

It is clear from the above literature that very few works have been reported in the published literature of nonlinear static behaviour of FG spherical panels. Based on the authors' knowledge, no work has been reported in literature for nonlinear bending behaviour of FG spherical shells by developing the nonlinear model in the framework of HSDT mid-plane kinematics and taking the geometric nonlinearity in Green-Lagrange sense. In addition to that, all the nonlinear higher order terms have been taken in the mathematical model for a more general approach. Hence, in this work authors have made an effort to develop general nonlinear mathematical model by taking the exact flexure of the shell panel and discretise the model using finite element steps. Finally, the nonlinear bending responses are obtained using a direct iterative method for the FG shell panel. It is worthy to mention that many industries are showing confidence on the simulation based model using the commercial available finite element (FE) software (ANSYS, LS Dyna and NASTRAN etc.) not only to reduce the computational time but also to reduce the experimental cost. The necessity of the present developed nonlinear model has been verified by comparing the responses with those available published results and corresponding simulation model developed in ANSYS parametric design language (APDL) code. In order to show the applicability of the present nonlinear model some related parametric (power law indices, curvature ratios, thickness ratios, support conditions, aspect ratios and load) studies have been carried out and discussed in detail.

2. Effective material properties of FGM

In this analysis, FG shell panels are assumed to vary continuously along their thickness direction based on a simple power-law distribution (Shen 2009), with volume fractions of each of the constituents. The sum of the volume fractions of ceramic (V_{f_c}) and the metal (V_{f_m}) is equal to unity for a unit volume.

$$V_{f_c} + V_{f_m} = 1 \tag{1}$$

The FGM's effective material property say, *P* is the functions of material properties and volume fractions of each constituent material which can be expressed by using simple mixture's rule of composite materials as in (Shen 2009).

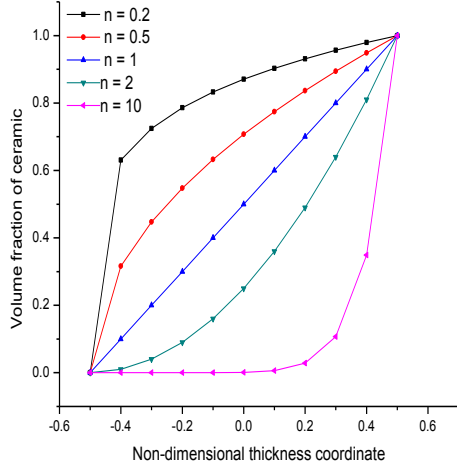$$P = P_c V_{f_c} + P_m V_{f_m} \tag{2}$$

Fig. 1 Variations of volume fraction of ceramic through non-dimensional thickness coordinate
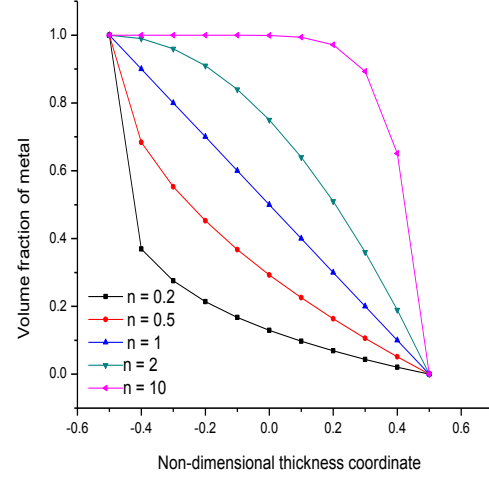
Fig. 2 Variations of volume fraction of metal through non-dimensional thickness coordinate

where, P_c and P_m are the material properties of ceramic and metal, respectively.

According to power-law distribution, the volume fractions of ceramic and metal can be represented as

$$\left. \begin{aligned} V_{f_c} &= \left(\frac{z}{h} + \frac{1}{2} \right)^n \\ V_{f_m} &= 1 - \left(\frac{z}{h} + \frac{1}{2} \right)^n \end{aligned} \right\} \tag{3}$$

where, n ($0 \leq n \leq \infty$) is the power-law index which characterizes the material variation through the thickness of the shell panel. The variations of volume fractions of the ceramic and the metal phase for different values of power-law indices ($n=0.2, 0.5, 1, 2$ and 10) along with the non-dimensional thickness coordinate ($Z=z/h$) are plotted in Figs. 1-2. It can be clearly seen that, ceramic content decreases with increase in power-law index values i.e., if $n=0$, the total material turns to ceramic and if $n=\infty$, it turns to metal.

The effective material property has been expressed using the Eqs. (1) - (3).

$$P = \left(P_c - P_m \right) \left(\frac{z}{h} + \frac{1}{2} \right)^n + P_m \tag{4}$$

Now, the Eq. (4) can be rewritten for the different material properties such as Young's modulus E and Poisson's ratio v

$$\left. \begin{aligned} E &= \left(E_c - E_m \right) \left(\frac{z}{h} + \frac{1}{2} \right)^n + E_m \\ v &= \left(v_c - v_m \right) \left(\frac{z}{h} + \frac{1}{2} \right)^n + v_m \end{aligned} \right\} \tag{5}$$

Table 1 Properties of the FGM constituents.

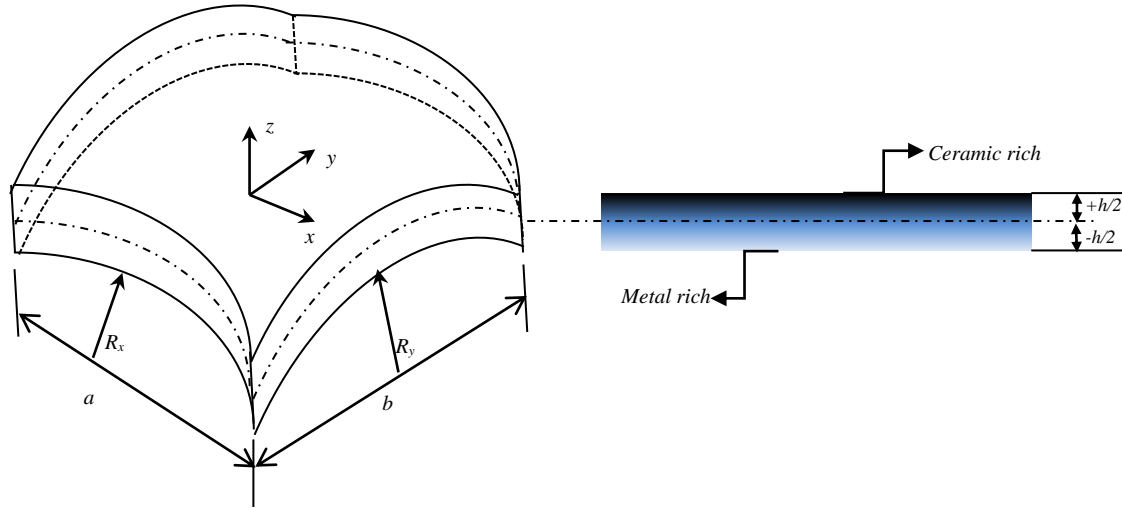| Materials	Properties		
	Young's Modulus E (GPa)	Poisson's Ratio v	Density ρ (Kg/m^3)
Aluminum (Al)	70	0.3	2707
Zirconia (ZrO$_2$)	151	0.3	3000

Fig. 3 Geometry and dimension of spherical FG shell panel

The properties of the FGM constituents at room temperature (300K) are mentioned in Table 1. These following properties are used throughout the analysis, if not stated otherwise.

3. General formulation

For the present analysis, a spherical FG shell panel of uniform thickness 'h' with sides a and b is considered as shown in Fig. 3. Here, R_x and R_y are the principal radii of curvatures of the shell panel along x and y directions, respectively. The principal radii of curvature of spherical panel is assumed as, $R_x=R_y=R$.

3.1 Kinematic model

The following HSDT displacement field is used for the FG shell panel to derive the mathematical model (Reddy 2003).

$$\left. \begin{array}{l} u(x,y,z) = u_0(x,y) + z\theta_x(x,y) + z^2 u_0^*(x,y) + z^3 \theta_x^*(x,y) \\ v(x,y,z) = v_0(x,y) + z\theta_y(x,y) + z^2 v_0^*(x,y) + z^3 \theta_y^*(x,y) \\ w(x,y,z) = w_0(x,y) \end{array} \right\} \quad (6)$$

where, u, v and w denote the displacements of a point along the (x, y, z) coordinates. u_0, v_0 and w_0 are corresponding displacements of a point on the mid-plane. θ_x and θ_y are the rotations of normal to the mid-plane about the y and x-axis, respectively. The functions u_0^*, v_0^*, θ_x^* and θ_y^* are the higher order terms in the Taylor series expansion defined in the mid-plane of the shell.

3.2 Strain displacement relations

The following equation defines the strain displacement relation which is commonly known as Green-Lagrange strain for any general material continuum

$$
\{\varepsilon\} = \begin{Bmatrix} \varepsilon_{xx} \\ \varepsilon_{yy} \\ \gamma_{xy} \\ \gamma_{xz} \\ \gamma_{yz} \end{Bmatrix} = \begin{Bmatrix} \left(\dfrac{\partial u}{\partial x} + \dfrac{w}{R_x}\right) \\[6pt] \left(\dfrac{\partial v}{\partial y} + \dfrac{w}{R_y}\right) \\[6pt] \left(\dfrac{\partial u}{\partial y} + \dfrac{\partial v}{\partial x} + \dfrac{2w}{R_{xy}}\right) \\[6pt] \left(\dfrac{\partial u}{\partial z} + \dfrac{\partial w}{\partial x} - \dfrac{u}{R_x}\right) \\[6pt] \left(\dfrac{\partial v}{\partial z} + \dfrac{\partial w}{\partial y} - \dfrac{v}{R_y}\right) \end{Bmatrix} + \begin{Bmatrix} \frac{1}{2}\left[\left(\dfrac{\partial u}{\partial x}+\dfrac{w}{R_x}\right)^2 + \left(\dfrac{\partial v}{\partial x}+\dfrac{w}{R_{xy}}\right)^2 + \left(\dfrac{\partial w}{\partial x}-\dfrac{u}{R_x}\right)^2\right] \\[6pt] \frac{1}{2}\left[\left(\dfrac{\partial u}{\partial y}+\dfrac{w}{R_{xy}}\right)^2 + \left(\dfrac{\partial v}{\partial y}+\dfrac{w}{R_y}\right)^2 + \left(\dfrac{\partial w}{\partial y}-\dfrac{v}{R_y}\right)^2\right] \\[6pt] \left[\left(\dfrac{\partial u}{\partial x}+\dfrac{w}{R_x}\right)\left(\dfrac{\partial u}{\partial y}+\dfrac{w}{R_{xy}}\right) + \left(\dfrac{\partial v}{\partial x}+\dfrac{w}{R_{xy}}\right)\left(\dfrac{\partial v}{\partial y}+\dfrac{w}{R_y}\right) + \left(\dfrac{\partial w}{\partial x}-\dfrac{u}{R_x}\right)\left(\dfrac{\partial w}{\partial y}-\dfrac{v}{R_y}\right)\right] \\[6pt] \left[\dfrac{\partial u}{\partial z}\left(\dfrac{\partial u}{\partial x}+\dfrac{w}{R_x}\right) + \dfrac{\partial v}{\partial z}\left(\dfrac{\partial v}{\partial x}+\dfrac{w}{R_{xy}}\right) + \dfrac{\partial w}{\partial z}\left(\dfrac{\partial w}{\partial x}-\dfrac{u}{R_x}\right)\right] \\[6pt] \left[\dfrac{\partial u}{\partial z}\left(\dfrac{\partial u}{\partial y}+\dfrac{w}{R_{xy}}\right) + \dfrac{\partial v}{\partial z}\left(\dfrac{\partial v}{\partial y}+\dfrac{w}{R_y}\right) + \dfrac{\partial w}{\partial z}\left(\dfrac{\partial w}{\partial y}-\dfrac{v}{R_y}\right)\right] \end{Bmatrix}
\tag{7}
$$

Eq. (7) can be presented as the sum of linear and nonlinear strains in the following manner

$$
\{\varepsilon\} = \{\varepsilon_L\} + \{\varepsilon_{NL}\}
\tag{8}
$$

By substituting Eq. (7) for Eq. (6), the strain vector is expressed as

$$
\varepsilon = \begin{Bmatrix} \varepsilon_{xx} \\ \varepsilon_{yy} \\ \gamma_{xy} \\ \gamma_{xz} \\ \gamma_{yz} \end{Bmatrix} = \begin{Bmatrix} \varepsilon_x^0 \\ \varepsilon_y^0 \\ \varepsilon_{xy}^0 \\ \varepsilon_{xz}^0 \\ \varepsilon_{yz}^0 \end{Bmatrix} + \begin{Bmatrix} \varepsilon_x^4 \\ \varepsilon_y^4 \\ \varepsilon_{xy}^4 \\ \varepsilon_{xz}^4 \\ \varepsilon_{yz}^4 \end{Bmatrix} + z\left[\begin{Bmatrix} k_x^1 \\ k_y^1 \\ k_{xy}^1 \\ k_{xz}^1 \\ k_{yz}^1 \end{Bmatrix} + \begin{Bmatrix} k_x^5 \\ k_y^5 \\ k_{xy}^5 \\ k_{xz}^5 \\ k_{yz}^5 \end{Bmatrix}\right] + z^2\left[\begin{Bmatrix} k_x^2 \\ k_y^2 \\ k_{xy}^2 \\ k_{xz}^2 \\ k_{yz}^2 \end{Bmatrix} + \begin{Bmatrix} k_x^6 \\ k_y^6 \\ k_{xy}^6 \\ k_{xz}^6 \\ k_{yz}^6 \end{Bmatrix}\right]
$$
$$
+ z^3\left[\begin{Bmatrix} k_x^3 \\ k_y^3 \\ k_{xy}^3 \\ k_{xz}^3 \\ k_{yz}^3 \end{Bmatrix} + \begin{Bmatrix} k_x^7 \\ k_y^7 \\ k_{xy}^7 \\ k_{xz}^7 \\ k_{yz}^7 \end{Bmatrix}\right] + z^4\begin{Bmatrix} k_x^8 \\ k_y^8 \\ k_{xy}^8 \\ k_{xz}^8 \\ k_{yz}^8 \end{Bmatrix} + z^5\begin{Bmatrix} k_x^9 \\ k_y^9 \\ k_{xy}^9 \\ k_{xz}^9 \\ k_{yz}^9 \end{Bmatrix} + z^6\begin{Bmatrix} k_x^{10} \\ k_y^{10} \\ k_{xy}^{10} \\ k_{xz}^{10} \\ k_{yz}^{10} \end{Bmatrix}
\tag{9}
$$

The above strain displacement relations (Eq. (9)) can be rearranged as

$$
\{\varepsilon\} = [T^l]\{\bar{\varepsilon}_l\} + [T^{nl}]\{\bar{\varepsilon}_{nl}\}
\tag{10}
$$

where, $\{\bar{\varepsilon}_l\} = \left\{ \varepsilon_x{}^0 \ \varepsilon_y{}^0 \ \varepsilon_{xy}{}^0 \ \varepsilon_{xz}{}^0 \ \varepsilon_{yz}{}^0 \ k_x{}^1 \ k_y{}^1 \ k_{xy}{}^1 \ k_{xz}{}^1 \ k_{yz}{}^1 \ k_x{}^2 \ k_y{}^2 \ k_{xy}{}^2 \ k_{xz}{}^2 \ k_{yz}{}^2 k_x{}^3 \ k_y{}^3 \ k_{xy}{}^3 \ k_{xz}{}^3 \ k_{yz}{}^3 \right\}^T$ and

$\{\bar{\varepsilon}_{nl}\} = \left\{ \begin{matrix} \varepsilon_x{}^4 \ \varepsilon_y{}^4 \ \varepsilon_{xy}{}^4 \ \varepsilon_{xz}{}^4 \ \varepsilon_{yz}{}^4 \ k_x{}^5 \ k_y{}^5 \ k_{xy}{}^5 \ k_{xz}{}^5 \ k_{yz}{}^5 \ k_x{}^6 \ k_y{}^6 \ k_{xy}{}^6 \ k_{xz}{}^6 \ k_{yz}{}^6 k_x{}^7 \ k_y{}^7 \ k_{xy}{}^7 \ k_{xz}{}^7 \ k_{yz}{}^7 \\ k_x{}^8 \ k_y{}^8 \ k_{xy}{}^8 \ k_{xz}{}^8 \ k_{yz}{}^8 \ k_x{}^9 \ k_y{}^9 \ k_{xy}{}^9 \ k_{xz}{}^9 \ k_{yz}{}^9 k_x{}^{10} \ k_y{}^{10} \ k_{xy}{}^{10} \ k_{xz}{}^{10} \ k_{yz}{}^{10} \end{matrix} \right\}^T$ are the linear and

nonlinear mid-plane strain vectors, defined in Appendix (A1). $[T^i]$ and $[T^{*i}]$ are the linear and the nonlinear thickness coordinate matrices, given in Appendix (A2).

3.3 Constitutive relations

The constitutive relations for any general FG shell panel is expressed as

$$\begin{Bmatrix} \sigma_{xx} \\ \sigma_{yy} \\ \tau_{xy} \\ \tau_{xz} \\ \tau_{yz} \end{Bmatrix} = \begin{bmatrix} Q_{11} & Q_{12} & 0 & 0 & 0 \\ Q_{21} & Q_{22} & 0 & 0 & 0 \\ 0 & 0 & Q_{66} & 0 & 0 \\ 0 & 0 & 0 & Q_{55} & 0 \\ 0 & 0 & 0 & 0 & Q_{44} \end{bmatrix} \begin{Bmatrix} \varepsilon_{xx} \\ \varepsilon_{yy} \\ \gamma_{xy} \\ \gamma_{xz} \\ \gamma_{yz} \end{Bmatrix} \tag{11}$$

where, $Q_{11} = Q_{22} = E/(1-\upsilon^2)$, $Q_{12} = Q_{21} = E*\upsilon/(1-\upsilon^2)$, $Q_{66} = Q_{55} = Q_{44} = E/2*(1+\upsilon)$

Eq. (11) can also be rewritten as

$$\{\sigma\} = \left[\bar{Q}\right]\{\varepsilon\} \tag{12}$$

where, $[\bar{Q}]$ is the reduced stiffness matrix.

3.4 Strain energy of the FG shell panel

The strain energy of the curved shell panel can be expressed as

$$U = \frac{1}{2}\int_v \{\varepsilon\}^T \{\sigma\} dV \tag{13}$$

Eq. (13) can be rewritten by substituting strains and stresses from Eqs. (10) and (12)

$$U = \frac{1}{2}\int_A \left(\{\bar{\varepsilon}_l\}^T [D_1]\{\bar{\varepsilon}_l\} + \{\bar{\varepsilon}_l\}^T [D_2]\{\bar{\varepsilon}_{nl}\} + \{\bar{\varepsilon}_{nl}\}^T [D_3]\{\bar{\varepsilon}_l\} + \{\bar{\varepsilon}_{nl}\}^T [D_4]\{\bar{\varepsilon}_{nl}\} \right) dA \tag{14}$$

where, $[D_1] = \int_{-h/2}^{+h/2} [T^l]^T [\bar{Q}][T^l] dz$, $[D_2] = \int_{-h/2}^{+h/2} [T^l]^T [\bar{Q}][T^{nl}] dz$, $[D_2] = \int_{-h/2}^{+h/2} [T^l]^T [\bar{Q}][T^{nl}] dz$ and

$[D_2] = \int_{-h/2}^{+h/2} [T^l]^T [\bar{Q}][T^{nl}] dz$.

3.5 Work done due to external transverse load

The work done by external applied load q is given by

$$W = \int_A \{\delta_0\}^T \{q\} dA \tag{15}$$

4. Finite element formulation

A nine noded isoparametric quadrilateral Lagrangian element with nine degrees of freedom per node is employed for the discretisation purpose. The displacement vector is expressed for each of the elements by

$$\{\delta_0\} = \sum_{i=1}^{9} N_i \{\delta_{0_i}\} \tag{16}$$

where, $\{\delta_{0_i}\} = \begin{bmatrix} u_{0_i} & v_{0_i} & w_{0_i} & \phi_{x_i} & \phi_{y_i} & u_{0_i}^* & v_{0_i}^* & \phi_{x_i}^* & \phi_{y_i}^* \end{bmatrix}$ is the nodal displacement vector at node i. N_i is the shape function for the ith node (Cook *et al*. 2009).

The linear and nonlinear mid-plane strain vector in terms of nodal displacement vector can be written as

$$\{\bar{\varepsilon}_l\} = [B]\{\delta_{0_i}\} \;,\; \{\bar{\varepsilon}_{nl}\} = [A][G]\{\delta_{0_i}\} \tag{17}$$

where, [B] is the product form of differential operators and the shape functions in the linear strain terms. [A] is the function of displacements and [G] is the product form of differential operator and shape functions in the nonlinear strain terms. [B], [A] and [G] matrices are mentioned in Appendix (A3)-(A5), respectively.

4.1 Governing equations

The final form of governing equation of FG shell panel is obtained using variational principle.

$$\delta \prod = \delta U - \delta W = 0 \tag{18}$$

where, δ is the variational symbol and $\prod$ is the total potential energy.

The equilibrium equation for the static analysis is obtained by substituting Eq. (18) for Eqs. (14)-(17) as follows

$$[K_s]\{\delta\} = \{q\} \tag{19}$$

where, $\{\delta\}$ is the global displacement and $[K_s]$ is the global stiffness matrix and it includes all the linear and the nonlinear stiffness matrices, $[K_1^l]$, $[K_1^{nl}]$, $[K_2^{nl}]$ and $[K_3^{nl}]$.

4.2 Solution techniques

The proposed and developed model has been solved using a homemade computer code in MATLAB environment and in ANSYS based on APDL code. The steps of solutions are discussed in detail in the following sections.

4.2.1 Solution techniques for HSDT model

The nonlinear static responses of FG shell panels are analysed through a finite element code in MATLAB which is based on the present mathematical model in the framework of the HSDT. The linear and nonlinear responses are obtained using direct iterative method and the steps are mentioned in Fig. 4.

Table 2 Different types of support condition

CCCC	$u_0=v_0=w_0=\theta_x=\theta_y=u_0^*=v_0^*=\theta_x^*=\theta_y^*=0$ at $x=0$, a and $y=0$, b
SSSS	$v_0=w_0=\theta_y=v_0^*=\theta_y^*=0$ at $x=0$, a ; $u_0=w_0=\theta_x=u_0^*=\theta_x^*=0$ at $y=0$, b
SCSC	$v_0=w_0=\theta_y=v_0^*=\theta_y^*=0$ at $x=0$, a; $u_0=v_0=w_0=\theta_x=\theta_y=u_0^*=v_0^*=\theta_x^*=\phi_y^*=0$ at $y=0$, b
HHHH	$u_0=v_0=w_0=\theta_y=v_0^*=\theta_y^*=0$ at $x=0$, a; $u_0=v_0=w_0=\theta_x=u_0^*=\theta_x^*=0$ at $y=0$, b

4.2.2 Solution steps in ANSYS model

A simulation model of FG panel is also developed in ANSYS environment using APDL code. The present ANSYS model is developed and discretised using an eight node serendipity element (SHELL281) with six degrees of freedom at each node. In this simulation model, the panel mid-plane kinematics is governed by the FSDT. The nonlinear solutions in ANSYS platform are obtained using Newton-Raphson method. The brief description on solution procedure in ANSYS platform are as follows:

1. As a first step, the geometry of the panel with sides a and b has been created.
2. Finite number of layers have been considered to emulate the FGM like material.
3. Each layer of the panel is assigned with calculated material properties according to the power-law distribution.
4. The created model has been discretised using SHELL281 element, from ANSYS element library, to obtain the required mesh.
5. Then, the boundary condition and the transverse uniformly distributed load are applied to obtain the required linear responses.
6. Finally, the nonlinear solutions are obtained by using Newton-Raphson method from in-built nonlinear solutions of ANSYS with a convergence tolerance ($\sim 10^{-3}$).

5 Results and discussions

The material properties are taken temperature independent and the details are given in Table 1. In order to avoid rigid body motion and to reduce the numbers of unknown from the final equations, there are few sets of constraint conditions either single or in combinations of clamped (C), simply-supported (S) and hinged (H) are employed throughout the computation as given in Table 2. For the analysis purpose, a uniformly distributed type of loading has been taken in the analysis. The following non-dimensional parameters are used throughout the analysis if not stated otherwise:

Central deflection, $\bar{w} = w / h$ and

Load parameter, $Q = (q / E_m)*(a / h)^4$.

5.1 Convergence behaviour of the FG panel

The nonlinear static behaviour of a simply-supported FG square shell panels are analysed under uniformly distributed load. The aluminum (Al) as the metal and zirconia (ZrO_2) as the ceramic

```
┌─────────────────────────────────────────┐
│  Initialising geometry, material properties │
└─────────────────────────────────────────┘
                    │
                    ▼
            ┌──────────────┐ ◄──────────────────┐
            │  Load steps  │                     │
            └──────────────┘                     │
                    │                            │
                    ▼                            │
            ┌──────────────┐                     │
            │ Iteration i = 0 │                  │
            └──────────────┘                     │
                    │                            │
                    ▼                            │
              ╱ i = i+1 ╲ ◄────────────┐         │
              ╲          ╱             │         │
                    │                  │         │
                    ▼                  │         │
      ┌──────────────────────────┐     │         │
      │ Initialising and Evaluating Elemental │  │
      │ stiffness matrix and force vector │    │  │
      └──────────────────────────┘     │         │
                    │                  │         │
                    ▼                  │         │
      ┌──────────────────────────┐     │         │
      │ Assembling global stiffness matrix │    │  │
      │      and force vector     │       │      │
      └──────────────────────────┘     │         │
                    │                  │         │
                    ▼                  │         │
      ┌──────────────────────────┐     │         │
      │ Solving and getting bending response │  │
      │ (1st iteration gives linear response) │  │
      └──────────────────────────┘     │         │
                    │                  │         │
                    ▼                  │         │
      ┌──────────────────────────┐     │         │
      │ Normalising and scaling the previous response │ │
      └──────────────────────────┘     │         │
                    │                  │         │
                    ▼                  │         │
      ┌──────────────────────────┐     │         │
      │ Updating the nonlinear global stiffness matrix │ │
      └──────────────────────────┘     │         │
                    │                  │         │
                    ▼                  │         │
      ┌──────────────────────────┐     │         │
      │ Solving and getting nonlinear response │   │
      └──────────────────────────┘     │         │
                    │                  │         │
                    ▼          No      │         │
              ╱ iᵗʰ−(i-1)ᵗʰ<10⁻³ ╲ ─────┘         │
              ╲                  ╱               │
                    │ Yes                        │
                    ▼                            │
            ┌──────────────┐                     │
            │ Print result │ ────────────────────┘
            └──────────────┘
```
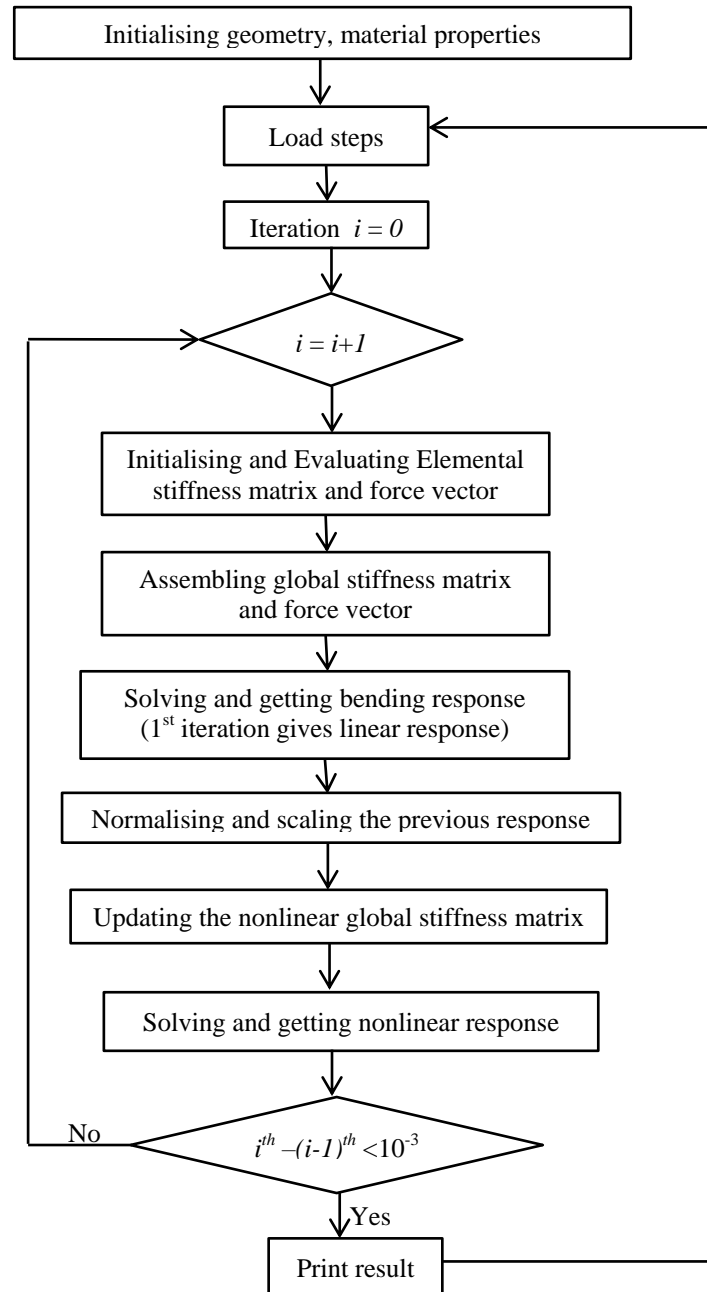
Fig. 4 A general procedure for nonlinear bending analysis of FG shell panel

material of the panel, respectively.

The convergence test has been done for simply-supported FG (Al/ZrO$_2$) flat panel (a/h=20) for n=0.5 and different load parameters. It is observed from Fig. 5 that the responses are converging well with the mesh refinement and a (5×5) mesh is sufficient to give the responses. Hence, a (5×5)

mesh has been used to obtain the responses for further analysis.

5.2 Comparison study FG flat/spherical panel

To check the efficacy of the present model as a first step the nonlinear bending responses obtained using the developed nonlinear model and compared with the published literature and the ANSYS values. In order to do so, the material and geometrical parameters are taken same as the previous problem as discussed in the convergence case. The results are compared with the flat panel results of Zhao and Liew (2009a) and the developed ANSYS model for different load parameters and the responses are shown in Fig. 6. It is well known that the flat panels are the simplest form of the shell panel. The non-dimensional central deflection values obtained using the present HSDT model are less in comparison with others because both the reference and ANSYS are based on FSDT kinematics which overestimates the responses as compared to the HSDT. It is interesting to note that the responses are almost linear for smaller values of load parameters.

In order to check the robustness of present model and to account the geometric nonlinearity, another problem has been carried out for a simply-supported square FG (Al/ZrO$_2$) spherical panel (R/a=5, a/h=20, n=1) with higher values of load parameter (Q=100, 200, 300, 400 and 500). The comparison between the present and the published results (Woo and Meguid 2001) is plotted in Fig. 7. The published results are based on the classical plate theory which neglects the shear strain terms because of that the differences between the published and the present results are comparatively large.

5.3 Numerical illustrations

In this section, numerical experimentations have been done for the present developed model
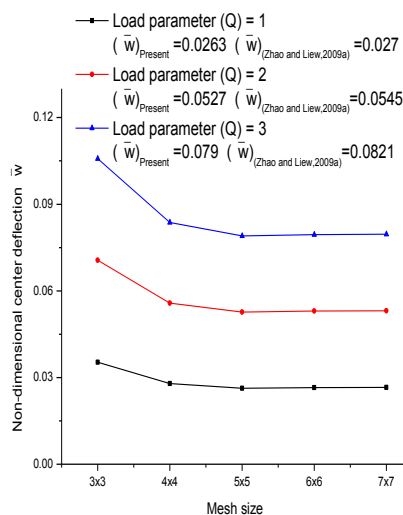
Fig. 5 Convergence study for non-dimensional central deflection of simply-supported FG (Al/ZrO$_2$) flat panel
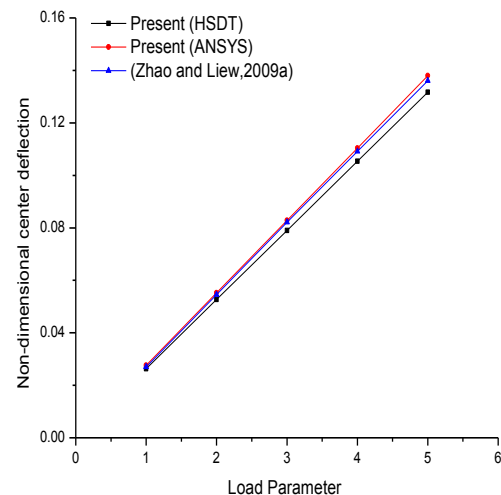
Fig. 6 Variation of non-dimensional central deflection with load parameters for simply-supported FG (Al/ZrO$_2$) flat panel
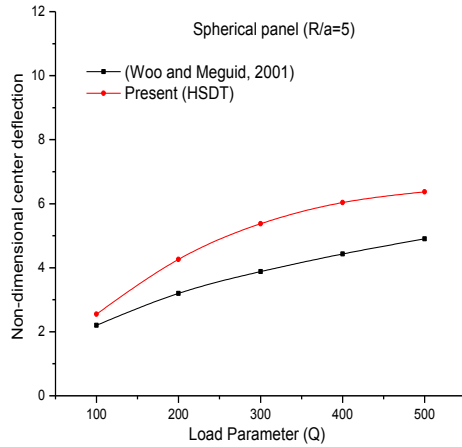
Fig. 7 Variation of non-dimensional central deflection with load parameters for simply-supported FG (Al/ZrO$_2$) spherical panel (*n*=1)
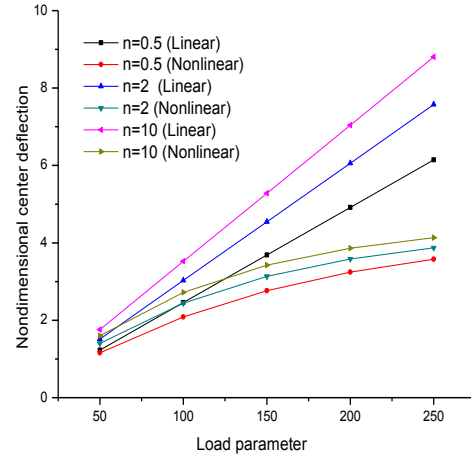

Fig. 8 Variation of non-dimensional central deflection with power-law indices and load parameters for simply-supported FG spherical (*R/a*=5) panel (*a/h*=10)

and the linear and the nonlinear bending behaviour of FG spherical shell panels for different parameters (power-law indices (*n*), thickness ratios (*a/h*), curvature ratios (*R/a*), aspect ratios (*a/b*), support conditions and load parameters) are exemplified.

It is well known that the gradation in FGM is based on the power law index value which decides the volume fraction of each constituent as well as the effective elastic constants. The effect of volume fraction of each (metal and ceramic) constituents on the stiffness of FG panel and the corresponding deflection behaviour have been analysed in this present example. Fig. 8 shows the non-dimensional central deflection of moderately thick (*a/h*=10) simply-supported square FG (Al/ZrO$_2$) spherical shell panel for five different load parameters (*Q*=50, 100, 150, 200 and 250) and three power-law indices (*n*=0.5, 2 and 10). It is observed that the non-dimensional central deflection increases with increase in power-law indices. It is because, as the *n* value increases the panel becomes metal rich and the stiffness value is lower than the ceramic. A similar type of behaviour can be observed from the present analysis.

The elastic properties of any FG structural components are the function of thickness and it will have a great influence on the overall structural stiffness. In order to examine the same, in this analysis the effect of thickness ratios (*a/h*=5, 10, 20 and 50) on the non-dimensional central deflections of a square simply-supported FG (Al/ZrO$_2$) spherical shell panel (*n*=2) is plotted in Fig. 9 using the same load parameters as mentioned in previous example. The both linear and the nonlinear non-dimensional central deflections are increased with increase in load parameter and decreased with increase in thickness ratio. It is also interesting to note that the effect of nonlinearity in thick FG spherical panel (*a/h*=5) is comparatively higher as compared to other cases.

It is true that the curved panels have higher membrane energy as compared to bending energy and degree of shallowness of any panel is being described in terms of its curvature. In order to address the effect of the curvature ratio on the bending behaviour an example has been solved and presented in Fig. 10. The figure presents the effect of curvature ratios (*R/a*=5, 10, 20 and 50) and
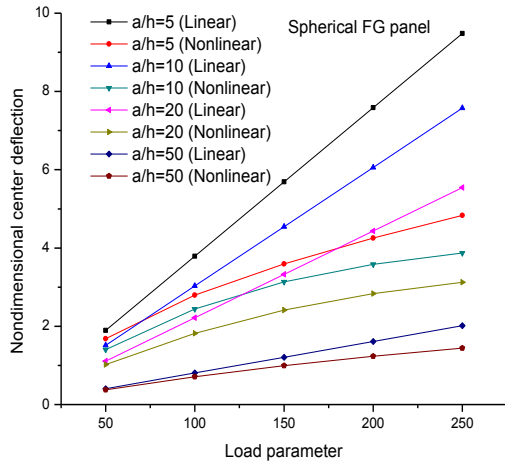
Fig. 9 Variation of non-dimensional central deflection with thickness ratios and load parameters for simply-supported FG spherical (*R/a*=5) panel (*n*=2)
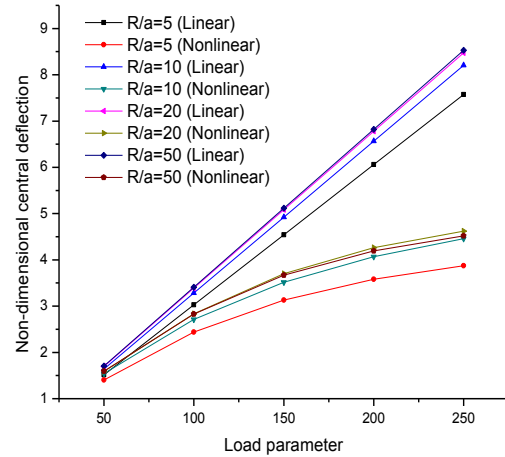

Fig. 10 Variation of non-dimensional central deflection with curvature ratios and load parameters for simply-supported FG spherical panel (*n*=2)
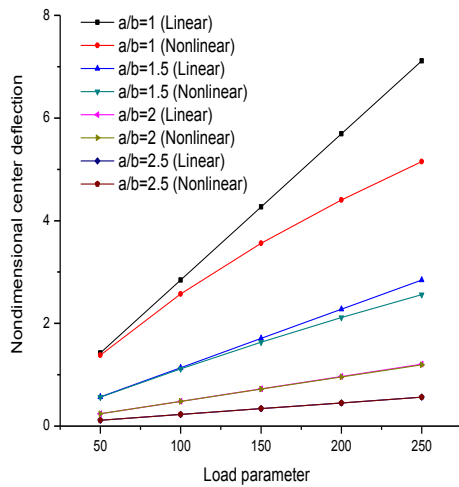

Fig. 11 Variation of non-dimensional central deflection with aspect ratios and load parameters for simply-supported FG spherical panel (*a/h*=100, *R/a*=50, *n*=2)
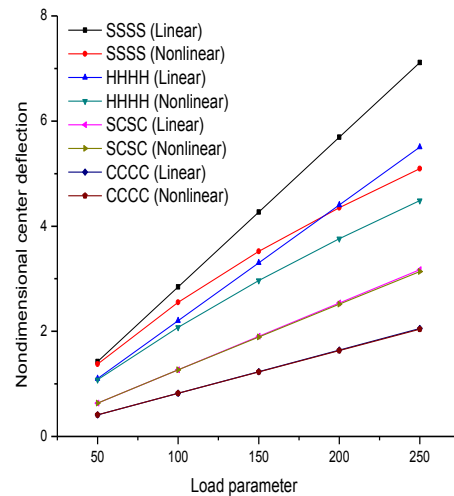

Fig. 12 Variation of non-dimensional central deflection with load parameters for different support conditions of square FG spherical panel (*a/h*=100, *R/a*=50, *n*=2)

load parameters on the non-dimensional central deflections of a simply-supported square FG (Al/ZrO$_2$) spherical panel (*n*=2, *a/h*=10). It is observed from the figure that the $\bar{w}$ increases with increase in curvature ratios. It is because of the fact that, as the curvature ratio increases the panel becomes flat and the bending behaviour follows the same line.

The aspect ratio is the deciding factor for any panel geometry which contributes to the stiffness calculation of the structure. Here, the variation of non-dimensional central deflection of simply-

supported FG (Al/ZrO$_2$) spherical panel (n=2, a/h=100, R/a=50) for four different aspect ratios (a/b=1, 1.5, 2 and 2.5) at five different load parameters (Q=50, 100, 150, 200 and 250) is presented in Fig. 11. The effects can clearly be seen in the figure that $\bar{w}$ decreases with increase in aspect ratios for both linear and nonlinear case. It also reveals that the differences between the linear and nonlinear responses are large in case of square FG panel i.e., at a/b=1 and the linear and nonlinear responses are almost same at higher values of aspect ratio i.e., at a/b=2 and 2.5.

The spatial degree of freedom is being removed from the structure to avoid the rigid body motion hence, in any analysis of deformable structure the model has to be well constrained. In addition to the above, the nature of support condition is also a major deciding parameter for final structural behaviour. Here, Fig. 12 presents the non-dimensional central deflection of square FG (Al/ZrO$_2$) spherical panel (n=2, a/h=100, R/a=50) for different type of support conditions (SSSS, CCCC, HHHH and SCSC) under the same loading conditions as discussed in previous example. It is observed that the deflection parameter increases as the number of constraints decreases i.e., the non-dimensional central deflections are lower for the clamped (CCCC) and higher for the simply-support (SSSS) cases. It is also noted that, the linear and nonlinear responses are nearly equal for CCCC and SCSC support conditions.

6. Conclusions

The nonlinear bending behaviour of functionally graded spherical shell panel is being analysed in this present article. The effective material properties of FG shell panels are graded in the thickness direction according to a power-law distribution of the volume fractions of the constituents. As a first step, a general nonlinear mathematical model for FG shell panel is developed based on the HSDT mid-plane kinematics by taking the geometric nonlinearity in Green-Lagrange sense. In addition to that, all the nonlinear higher order terms are considered in the present nonlinear model to achieve a general case. The shell model is discretised using a nine noded isoparametric Lagrangian element with nine degrees of freedom per node and the governing differential equation is derived using variational principle. The model is validated by comparing the bending responses obtained using the presently developed nonlinear mathematical model with commercial FE tool (ANSYS) as well as the other available published literatures. The efficacy and generality of the developed nonlinear model has been checked by evaluating the responses for different parameters such as the power-law indices, the thickness ratios, the aspect ratios, the support conditions and the curvature ratios. Finally, some conclusions have been drawn based on the parametric study of FG spherical panels and discussed point wise in the following lines.

• The linear and nonlinear central deflection increase with increase in the power-law indices and the curvature ratios.

• The linear and nonlinear central deflection decrease with increase in the thickness ratios and the aspect ratios.

• It is interesting to note that as the number of boundary constraints increases, the $\bar{w}$ decreases and the effect of nonlinearity is dominant in case of less number of constraints i.e., in simply-supported condition in comparison to other types of support conditions.

• It is also understood from the present analysis that the FG spherical shell panel exhibits a hardening type of nonlinear behaviour.

References

Alijani, F. and Amabili, M. (2014), "Non-linear vibrations of shells: a literature review from 2003 to 2013", *Int. J. Nonlin. Mech.*, **58**, 233-257.

Bian, Z.G., Ying, J., Chen, W.Q. and Ding, H.J. (2006), "Bending and free vibration analysis of a smart functionally graded plate", *Struct. Eng. Mech.*, **23**(1), 97-113.

Bich, D.H. and Tung, H.V. (2011), "Non-linear axisymmetric response of functionally graded shallow spherical shells under uniform external pressure including temperature effects", *Int. J. Nonlin. Mech.*, **46**, 1195-1204.

Bich, D.H., Dung, D.V. and Hoa, L.K. (2012), "Nonlinear static and dynamic buckling analysis of functionally graded shallow spherical shells including temperature effects", *Compos. Struct.*, **94**, 2952-2960.

Birman, V. and Byrd, L.W. (2007), "Modeling and analysis of functionally graded materials and structures", *Appl. Mech. Rev.*, **60**, 195-216.

Cook, R.D., Malkus, D.S., Plesha, M.E. and Witt, R.J. (2009), *Concepts and applications of finite element analysis*, 4th Edition, John Wiley & Sons Pvt. Ltd., Singapore.

Jha, D.K., Kant, T., Singh, R.K. (2013), "A critical review of recent research on functionally graded plates", Compos. Struct., **96,** 833-849.

Lei, Z.X., Zhang, L.W., Liew, K.M. and Yu, J.L. (2014), "Dynamic stability analysis of carbon nanotube-reinforced functionally graded cylindrical panels using the element-free kp-Ritz method", *Compos. Struct.*, **113**, 328-338.

Liew, K.M., Lei, Z.X., Yu, J.L. and Zhang, L.W. (2014), "Postbuckling of carbon nanotube-reinforced functionally graded cylindrical panels under axial compression using a meshless approach", *Comput. Meth. Appl. Mech. Eng.*, **268**, 1-17.

Liew, K.M., Zhao, X., Ferreira, A.J.M. (2011), "A review of meshless methods for laminated and functionally graded plates and shells", *Compos. Struct.*, **93**(8), 2031-2041.

Mantari, J.L., Oktem, A.S. and Soares, C.G. (2012), "Bending response of functionally graded plates by using a new higher order shear deformation theory", *Compos. Struct.*, **94**, 714-723.

Mao, Y.Q., Fu, Y.M., Chen, C.P. and Li, Y.L. (2011), "Nonlinear dynamic response for functionally graded shallow shell under low velocity impact in thermal environment", *Appl. Math. Model.*, **35**, 2887-2900.

Navazi, H.M. and Haddadpour, H. (2008), "Nonlinear cylindrical bending analysis of shear deformable functionally graded plates under different loadings using analytical methods", "*Int. J. Mech. Sci.*, **50**, 1650-1657.

Neves, A.M.A., Ferreira, A.J.M., Carrera, E., Cinefra, M., Roque, C.M.C., Jorge, R.M.N. and Soares, C.M.M. (2011), "Bending of FGM plates by a sinusoidal plate formulation and collocation with radial basis functions", *Mech. Res. Commun.*, **38**, 368-371.

Neves, A.M.A., Ferreira, A.J.M., Carrera, E., Cinefra, M., Roque, C.M.C., Jorge, R.M.N. and Soares, C.M.M. (2012), "A quasi-3D hyperbolic shear deformation theory for the static and free vibration analysis of functionally graded plates", *Compos. Struct.*, **94**, 1814-1825.

Oktem, A.S., Mantari, J.L. and Soares, C.G. (2012), "Static response of functionally graded plates and doubly-curved shells based on a higher order shear deformation theory", *Eur. J. Mech. A-Solid.*, **36**, 163-172.

Reddy, J.N. (2003), *Mechanics of laminated composite: Plates and shells-Theory and analysis*, 2nd Edition, CRC press, Boca Raton, FL.

Santos, H., Soares, C.M.M., Soares, C.A.M. and Reddy, J.N. (2009), "A semi-analytical finite element model for the analysis of cylindrical shells made of functionally graded materials", *Compos. Struct.*, **91**, 427-432.

Shen H.S. (2009), *Functionally graded material: Nonlinear analysis of plates & shells*, CRC press, Boca Raton, FL.

Shen, H.S. (2002), "Nonlinear bending response of functionally graded plates subjected to transverse loads

and in thermal environments", *Int. J. Mech. Sci.*, **44**, 561-584.

Talha, M. and Singh, B.N. (2010), "Static response and free vibration analysis of FGM plates using higher order shear deformation theory", *Appl. Math. Model.*, **34**, 3991-4011.

Thai, H.T. and Kim, S.E. (2013), "A simple higher-order shear deformation theory for bending and free vibration analysis of functionally graded plates", *Compos. Struct.*, **96**, 165-173.

Woo, J. and Meguid, S.A. (2001), "Nonlinear analysis of functionally graded plates and shallow shells", *Int. J. Solid. Struct.*, **38**, 7409-7421.

Xiang, S. and Kang G. (2013), "A nth-order shear deformation theory for the bending analysis on the functionally graded plates", *Eur. J. Mech. A-Solid.*, **37**, 336-343.

Zenkour, A.M. and Sobhy, M. (2013), "Dynamic bending response of thermoelastic functionally graded plates resting on elastic foundations", *Aerosp. Sci. Technol.*, **29**, 7-17.

Zhang, L.W., Lei, Z.X., Liew, K.M. and Yu, J.L. (2014a), "Static and dynamic of carbon nanotube reinforced functionally graded cylindrical panels", *Compos. Struct.*, **111**, 205-212.

Zhang, L.W., Lei, Z.X., Liew, K.M. and Yu, J.L. (2014b), "Large deflection geometrically nonlinear analysis of carbon nanotube-reinforced functionally graded cylindrical panels", *Comput. Meth. Appl. Mech. Eng.*, **273**, 1-18.

Zhang, L.W., Zhu, P. and Liew, K.M. (2014), "Thermal buckling of functionally graded plates using a local Kriging meshless method", *Compos. Struct.*, **108**, 472-492.

Zhao, X. and Liew, K.M. (2009a), "Geometrically nonlinear analysis of functionally graded plates using the element-free kp-Ritz method", *Comput. Meth. Appl. Mech. Eng.*, **198**, 2796-2811.

Zhao, X. and Liew, K.M. (2009b), "Geometrically nonlinear analysis of functionally graded shells", *Int. J. Mech. Sci.*, **51**, 131-144.

Zhao, X., Lee, Y.Y. and Liew, K.M. (2009), "Thermoelastic and vibration analysis of functionally graded cylindrical shells", *Int. J. Mech. Sci.*, **51**, 694-707.

Zhu, P., Zhang, L.W. and Liew, K.M. (2014), "Geometrically nonlinear thermomechanical analysis of moderately thick functionally graded plates using a local Petrov-Galerkin approach with moving Kriging interpolation", *Compos. Struct.*, **107**, 298-314.

PL

Appendix

Linear mid-plane strain terms

$$\varepsilon_x^0 = u_{,x}, \ \varepsilon_y^0 = v_{,y}, \ \varepsilon_{xy}^0 = u_{,y} + v_{,x}, \ \varepsilon_{xz}^0 = w_{,x} + \theta_x, \ \varepsilon_{yz}^0 = w_{,y} + \theta_y, \ k_x^1 = \theta_{x,x}, \ k_y^1 = \theta_{y,y}, \ k_{xy}^1 = \theta_{x,y} + \theta_{y,x},$$

$$k_{xz}^1 = 2u_0^* - \theta_x / R_x, \ k_{yz}^1 = 2v_0^* - \theta_y / R_y, \ k_x^2 = u_{0,x}^*, \ k_y^2 = v_{0,y}^*, \ k_{xy}^2 = u_{0,y}^* + v_{0,x}^*, \ k_{xz}^2 = 3\theta_x^* - u_0^* / R_x,$$

$$k_{yz}^2 = 3\theta_y^* - v_0^* / R_y, \ k_x^3 = \theta_{x,x}^*, \ k_y^3 = \theta_{y,y}^*, \ k_{xy}^3 = \theta_{x,y}^* + \theta_{y,x}^*, \ k_{xz}^3 = -\theta_x^* / R_x, \ k_{yz}^3 = -\theta_y^* / R_y.$$

Nonlinear mid-plane strain terms

$$\varepsilon_x^4 = \tfrac{1}{2}u_{,x}^2 + \tfrac{1}{2}v_{,x}^2 + \tfrac{1}{2}w_{,x}^2, \ \varepsilon_y^4 = \tfrac{1}{2}u_{,y}^2 + \tfrac{1}{2}v_{,y}^2 + \tfrac{1}{2}w_{,y}^2, \ \varepsilon_{xy}^4 = u_{,x}u_{,y} + v_{,x}v_{,y} + w_{,x}w_{,y}, \ \varepsilon_{xz}^4 = u_{,x}\theta_y + v_{,x}\theta_y$$

$$k_x^5 = u_{,x}\theta_{x,x} + v_{,x}\theta_{y,x} - w_{,x}\theta_x / R_x \ , \ k_y^5 = u_{,x}\theta_{x,y} + v_{,y}\theta_{y,y} - w_{,y}\theta_y / R_y$$

$$k_{xy}^5 = u_{,x}\theta_{x,y} + u_{,y}\theta_{x,x} + v_{,x}\theta_{y,y} + v_{,y}\theta_{y,x} - w_{,x}\theta_y / R_y - w_{,y}\theta_x / R_x \ , \ k_{xz}^5 = 2u_{,x}u_0^* + 2v_{,x}v_0^* + \theta_{x,x}\theta_x + \theta_{y,x}\theta_y$$

$$k_{yz}^5 = 2u_{,y}u_0^* + 2v_{,y}v_0^* + \theta_{x,x}\theta_x + \theta_{y,y}\theta_y \qquad k_x^6 = u_{,x}u_{0,x}^* + v_{,x}v_{0,x}^* - w_{,x}u_0^* / R_x + \tfrac{1}{2}\theta_{x,x}^2 + \tfrac{1}{2}\theta_{y,x}^2 + \tfrac{1}{2}\theta_x^2 / R_x^2$$

$$k_y^6 = u_{,y}u_{0,y}^* + v_{,y}v_{0,y}^* - w_{,y}v_0^* / R_y + \tfrac{1}{2}\theta_{x,y}^2 + \tfrac{1}{2}\theta_{y,y}^2 + \tfrac{1}{2}\theta_y^2 / R_y^2$$

$$k_{xy}^6 = u_{,x}u_{0,y}^* + u_{,y}u_{0,x}^* + v_{,x}v_{0,y}^* + v_{,y}v_{0,x}^* - w_{,x}v_0^*/R_y - w_{,y}u_0^*/R_x + \theta_{x,x}\theta_{x,y} + \theta_{y,x}\theta_{y,y} + \theta_x\theta_y / R_x R_y$$

$$k_{xz}^6 = 3u_{,x}\theta_x^* + 3v_{,x}\theta_y^* + 2\theta_{x,x}u_0^* + 2\theta_{y,x}v_0^* + u_{0,x}^*\theta_x + v_{0,x}^*\theta_y$$

$$k_{yz}^6 = 3u_{,y}\theta_x^* + 3v_{,y}\theta_y^* + 2\theta_{x,y}u_0^* + 2\theta_{y,y}v_0^* + u_{0,y}^*\theta_x + v_{0,y}^*\theta_y$$

$$k_x^7 = u_{,x}\theta_{x,x}^* + v_{,x}\theta_{y,x}^* - w_{,x}\theta_x^* / R_x + \theta_{x,x}u_{0,x}^* + \theta_{y,x}v_{0,x}^* + \theta_x u_0^* / R_x^2$$

$$k_y^7 = u_{,y}\theta_{x,y}^* + v_{,y}\theta_{y,y}^* - w_{,y}\theta_y^* / R_y + \theta_{x,y}u_{0,y}^* + \theta_{y,y}v_{0,y}^* + \theta_y v_0^* / R_y^2$$

$$k_{xy}^7 = u_{,x}\theta_{x,y}^* + u_{,y}\theta_{x,x}^* + v_{,x}\theta_{y,y}^* + v_{,y}\theta_{y,x}^* - w_{,x}\theta_y^* / R_y - w_{,y}\theta_x^* / R_x + \theta_{x,x}u_{0,y}^* + \theta_{x,y}u_{0,x}^* + \theta_{y,x}v_{0,y}^*$$
$$+ \theta_{y,y}v_{0,x}^* + \theta_x v_0^* / R_x R_y + \theta_y u_0^* / R_x R_y$$

$$k_{xz}^7 = 3\theta_{x,x}\theta_x^* + 3\theta_{y,x}\theta_y^* + 2u_{0,x}^*u_0^* + 2v_{0,x}^*v_0^* + \theta_{x,x}^*\theta_x + \theta_{y,x}^*\theta_y$$

$$k_{yz}^7 = 3\theta_{x,y}\theta_x^* + 3\theta_{y,y}\theta_y^* + 2u_{0,y}^*u_0^* + 2v_{0,y}^*v_0^* + \theta_{x,y}^*\theta_x + \theta_{y,y}^*\theta_y$$

$$k_x^8 = \theta_{x,x}\theta_{x,x}^* + \theta_{y,x}\theta_{y,x}^* + \tfrac{1}{2}(u_{0,x}^*)^2 + \tfrac{1}{2}(v_{0,x}^*)^2 + \theta_x\theta_x^* / R_x^2 + \tfrac{1}{2}(u_0^* / R_x)^2$$

$$k_y^8 = \theta_{x,y}\theta_{x,y}^* + \theta_{y,y}\theta_{y,y}^* + \tfrac{1}{2}(u_{0,y}^*)^2 + \tfrac{1}{2}(v_{0,y}^*)^2 + \theta_y\theta_y^* / R_y^2 + \tfrac{1}{2}(v_0^* / R_y)^2$$

$$k_{xy}^8 = \theta_{x,x}\theta_{x,y}^* + \theta_{x,y}\theta_{x,x}^* + \theta_{y,x}\theta_{y,y}^* + \theta_{y,y}\theta_{y,x}^* + u_{0,x}^*u_{0,y}^* + v_{0,x}^*v_{0,y}^* + \theta_x\theta_y^* / R_x R_y + \theta_y\theta_x^* / R_x R_y + u_0^*v_0^* / R_x R_y$$

$$k_{xz}^8 = 3u_{0,x}^*\theta_x^* + 3v_{0,x}^*\theta_y^* + 2\theta_{x,x}^*u_0^* + 2\theta_{y,x}^*v_0^* \ , \ k_{yz}^8 = 3u_{0,y}^*\theta_x^* + 3v_{0,y}^*\theta_y^* + 2\theta_{x,y}^*u_0^* + 2\theta_{y,y}^*v_0^*$$

$$k_x^9 = u_{0,x}^*\theta_{x,x}^* + u_{0,y}^*\theta_{x,x}^* + v_{0,x}^*\theta_{y,y}^* + v_{0,y}^*\theta_{y,x}^* + u_0^*\theta_y^* / R_x R_y + v_0^*\theta_x^* / R_x R_y \ , \ k_{xz}^9 = 3\theta_{x,x}^*\theta_x^* + 3\theta_{y,x}^*\theta_y^*$$

$$k_{xy}^9 = u_{0,x}^*\theta_{x,y}^* + u_{0,y}^*\theta_{x,x}^* + v_{0,x}^*\theta_{y,y}^* + v_{0,y}^*\theta_{y,x}^* + u_0^*\theta_y^*/R_x R_y + v_0^*\theta_x^*/R_x R_y \ , \ k_{xz}^9 = 3\theta_{x,x}^*\theta_x^* + 3\theta_{y,x}^*\theta_y^*$$

$$k_{yz}^9 = 3\theta_{x,y}^*\theta_x^* + 3\theta_{y,y}^*\theta_y^* \ , \ k_x^{10} = \tfrac{1}{2}(\theta_{x,x}^*)^2 + \tfrac{1}{2}(\theta_{y,x}^*)^2 + \tfrac{1}{2}(\theta_x^* / R_x)^2 \ , \ k_y^{10} = \tfrac{1}{2}(\theta_{x,y}^*)^2 + \tfrac{1}{2}(\theta_{y,y}^*)^2 + \tfrac{1}{2}(\theta_y^* / R_y)^2$$

$$k_{xy}^{10} = \theta_{x,x}^*\theta_{x,y}^* + \theta_{y,x}^*\theta_{y,y}^* + \theta_x^*\theta_y^*/R_x R_y.$$

where, $u_{,x} = \partial u_0 / \partial x + w_0 / R_x$, $u_{,y} = \partial u_0 / \partial y + w_0 / R_{xy}$, $v_{,x} = \partial v_0 / \partial x + w_0 / R_{xy}$, $v_{,y} = \partial v_0 / \partial y + w_0 / R_y$,
$w_{,x} = \partial w_0 / \partial x - u_0 / R_x$, $w_{,y} = \partial w_0 / \partial y - v_0 / R_y$.

(A1)

Linear thickness coordinate matrix

$$
\left[T^{l}\right]_{5\times20} =
\begin{bmatrix}
1 & 0 & 0 & 0 & 0 & z & 0 & 0 & 0 & 0 & z^2 & 0 & 0 & 0 & 0 & z^3 & 0 & 0 & 0 & 0 \\
0 & 1 & 0 & 0 & 0 & 0 & z & 0 & 0 & 0 & 0 & z^2 & 0 & 0 & 0 & 0 & z^3 & 0 & 0 & 0 \\
0 & 0 & 1 & 0 & 0 & 0 & 0 & z & 0 & 0 & 0 & 0 & z^2 & 0 & 0 & 0 & 0 & z^3 & 0 & 0 \\
0 & 0 & 0 & 1 & 0 & 0 & 0 & 0 & z & 0 & 0 & 0 & 0 & z^2 & 0 & 0 & 0 & 0 & z^3 & 0 \\
0 & 0 & 0 & 0 & 1 & 0 & 0 & 0 & 0 & z & 0 & 0 & 0 & 0 & z^2 & 0 & 0 & 0 & 0 & z^3
\end{bmatrix}
$$

Nonlinear thickness coordinate matrix

$$
\left[T^{nl}\right]_{5\times35} =
\begin{bmatrix}
1 & 0 & 0 & 0 & 0 & z & 0 & 0 & 0 & 0 & z^2 & 0 & 0 & 0 & 0 & z^3 & 0 & 0 & 0 & 0 \\
0 & 1 & 0 & 0 & 0 & 0 & z & 0 & 0 & 0 & 0 & z^2 & 0 & 0 & 0 & 0 & z^3 & 0 & 0 & 0 \\
0 & 0 & 1 & 0 & 0 & 0 & 0 & z & 0 & 0 & 0 & 0 & z^2 & 0 & 0 & 0 & 0 & z^3 & 0 & 0 \\
0 & 0 & 0 & 1 & 0 & 0 & 0 & 0 & z & 0 & 0 & 0 & 0 & z^2 & 0 & 0 & 0 & 0 & z^3 & 0 \\
0 & 0 & 0 & 0 & 1 & 0 & 0 & 0 & 0 & z & 0 & 0 & 0 & 0 & z^2 & 0 & 0 & 0 & 0 & z^3
\end{bmatrix}
$$

(A2)

$$
\begin{bmatrix}
z^4 & 0 & 0 & 0 & 0 & z^5 & 0 & 0 & 0 & 0 & z^6 & 0 & 0 & 0 & 0 \\
0 & z^4 & 0 & 0 & 0 & 0 & z^5 & 0 & 0 & 0 & 0 & z^6 & 0 & 0 & 0 \\
0 & 0 & z^4 & 0 & 0 & 0 & 0 & z^5 & 0 & 0 & 0 & 0 & z^6 & 0 & 0 \\
0 & 0 & 0 & z^4 & 0 & 0 & 0 & 0 & z^5 & 0 & 0 & 0 & 0 & z^6 & 0 \\
0 & 0 & 0 & 0 & z^4 & 0 & 0 & 0 & 0 & z^5 & 0 & 0 & 0 & 0 & z^6
\end{bmatrix}
$$

Individual terms of matrix [B]

$[B]_{1,1} = \partial/\partial x$, $[B]_{1,3} = 1/R_x$, $[B]_{2,2} = \partial/\partial y$, $[B]_{2,3} = 1/R_y$, $[B]_{3,1} = \partial/\partial y$, $[B]_{3,2} = \partial/\partial x$, $[B]_{3,3} = 2/R_{xy}$,

$[B]_{4,1} = -1/R_x$, $[B]_{4,3} = \partial/\partial x$, $[B]_{4,4} = 1$, $[B]_{5,2} = -1/R_y$, $[B]_{5,3} = \partial/\partial x$, $[B]_{5,5} = 1$, $[B]_{6,4} = \partial/\partial x$,

$[B]_{7,5} = \partial/\partial y$, $[B]_{8,4} = \partial/\partial y$, $[B]_{8,5} = \partial/\partial x$, $[B]_{9,4} = -1/R_x$, $[B]_{9,6} = 2$, $[B]_{10,5} = -1/R_y$, $[B]_{10,7} = 2$,

$[B]_{11,6} = \partial/\partial x$, $[B]_{12,7} = \partial/\partial y$, $[B]_{13,6} = \partial/\partial y$, $[B]_{13,7} = \partial/\partial x$, $[B]_{14,6} = -1/R_x$, $[B]_{14,8} = 2$, $[B]_{15,7} = -1/R_y$, $[B]_{15,9} = 2$, $[B]_{16,8} = \partial/\partial x$, $[B]_{17,9} = \partial/\partial y$, $[B]_{18,8} = \partial/\partial y$, $[B]_{18,9} = \partial/\partial x$, $[B]_{19,8} = -1/R_x$,

$[B]_{20,9} = -1/R_y$. (A3)

Individual terms of matrix [A]

$[A]_{1,1} = \tfrac{1}{2} u_{,x}$, $[A]_{1,3} = \tfrac{1}{2} v_{,x}$, $[A]_{1,5} = \tfrac{1}{2} w_{,x}$, $[A]_{2,2} = \tfrac{1}{2} u_{,y}$, $[A]_{2,4} = \tfrac{1}{2} v_{,y}$, $[A]_{2,6} = \tfrac{1}{2} w_{,y}$, $[A]_{3,1} = u_{,y}$, $[A]_{3,3} = v_{,y}$, $[A]_{3,5} = w_{,y}$, $[A]_{4,1} = \theta_x$, $[A]_{4,3} = \theta_y$, $[A]_{5,2} = \theta_x$, $[A]_{5,4} = \theta_y$, $[A]_{6,1} = \theta_{x,x}$, $[A]_{6,3} = \theta_{y,x}$,

$[A]_{6,5} = -\theta_x/R_x$, $[A]_{7,2} = \theta_{x,y}$, $[A]_{7,4} = \theta_{y,y}$, $[A]_{7,6} = -\theta_y/R_y$, $[A]_{8,1} = \theta_{x,y}$, $[A]_{8,2} = \theta_{x,x}$, $[A]_{8,3} = \theta_{y,y}$, $[A]_{8,4} = \theta_{y,x}$, $[A]_{8,5} = -\theta_y/R_y$, $[A]_{8,6} = -\theta_x/R_x$, $[A]_{9,1} = 2u_0^*$, $[A]_{9,3} = 2v_0^*$, $[A]_{9,7} = \theta_x$, $[A]_{9,9} = \theta_y$,

$[A]_{10,2} = 2u_0^*$, $[A]_{10,4} = 2v_0^*$, $[A]_{10,8} = \theta_x$, $[A]_{10,10} = \theta_y$, $[A]_{11,1} = u_{0,x}^*$, $[A]_{11,3} = v_{0,x}^*$, $[A]_{11,5} =$

$-u_0^* / R_x$, $[A]_{11,7} = \tfrac{1}{2}\,\theta_{x,x}$, $[A]_{11,9} = \tfrac{1}{2}\,\theta_{y,x}$, $[A]_{12,2} = u_{0,y}^*$, $[A]_{12,4} = v_{0,y}^*$, $[A]_{12,6} = -v_0^* / R_y$, $[A]_{12,8} =$

$\tfrac{1}{2}\,\theta_{x,y}$, $[A]_{12,10} = \tfrac{1}{2}\,\theta_{y,y}$, $[A]_{13,1} = u_{0,y}^*$, $[A]_{13,2} = u_{0,x}^*$, $[A]_{13,3} = v_{0,y}^*$, $[A]_{13,4} = v_{0,x}^*$, $[A]_{13,5} = -v_0^* / R_y$,

$[A]_{13,6} = -u_0^* / R_x$, $[A]_{13,7} = \theta_{x,y}$, $[A]_{13,9} = \theta_{y,y}$, $[A]_{14,1} = 3\theta_x^*$, $[A]_{14,3} = 3\theta_y^*$, $[A]_{14,7} = 2u_0^*$, $[A]_{14,9} =$

$2v_0^*$, $[A]_{14,11} = \theta_x$, $[A]_{14,13} = \theta_y$, $[A]_{15,2} = 3\theta_x^*$, $[A]_{15,4} = 3\theta_y^*$, $[A]_{15,8} = 2u_0^*$, $[A]_{15,10} = 2v_0^*$, $[A]_{15,12}$

$= \theta_x$, $[A]_{15,14} = \theta_y$, $[A]_{16,1} = \theta_{x,x}^*$, $[A]_{16,3} = \theta_{y,x}^*$, $[A]_{16,5} = -\theta_x^* / R_x$, $[A]_{16,7} = u_{0,x}^*$, $[A]_{16,9} = v_{0,x}^*$,

$[A]_{16,19} = u_0^* / R_x^2$, $[A]_{17,2} = \theta_{x,y}^*$, $[A]_{17,4} = \theta_{y,y}^*$, $[A]_{17,6} = -\theta_y^* / R_y$, $[A]_{17,8} = u_{0,y}^*$, $[A]_{17,10} = v_{0,y}^*$,

$[A]_{17,20} = v_0^* / R_y^2$, $[A]_{18,1} = \theta_{x,y}^*$, $[A]_{18,2} = \theta_{x,x}^*$, $[A]_{18,3} = \theta_{y,y}^*$, $[A]_{18,4} = \theta_{y,x}^*$, $[A]_{18,5} = -\theta_y^* / R_y$,

$[A]_{18,6} = -\theta_x^* / R_x$, $[A]_{18,7} = u_{0,y}^*$, $[A]_{18,8} = u_{0,x}^*$, $[A]_{18,9} = v_{0,y}^*$, $[A]_{18,10} = v_{0,x}^*$, $[A]_{18,19} = v_0^* / R_x R_y$,

$[A]_{18,20} = u_0^* / R_x R_y$, $[A]_{19,7} = 3\theta_x^*$, $[A]_{19,9} = 3\theta_y^*$, $[A]_{19,11} = 2u_0^*$, $[A]_{19,13} = 2v_0^*$, $[A]_{19,15} = \theta_x$,

$[A]_{19,17} = \theta_y$, $[A]_{20,8} = 3\theta_x^*$, $[A]_{20,10} = 3\theta_y^*$, $[A]_{20,12} = 2u_0^*$, $[A]_{20,14} = 2v_0^*$, $[A]_{20,16} = \theta_x$, $[A]_{20,18} = \theta_y$,

$[A]_{21,7} = \theta_{x,x}^*$, $[A]_{21,9} = \theta_{y,x}^*$, $[A]_{21,11} = \tfrac{1}{2}\,u_{0,x}^*$, $[A]_{21,13} = \tfrac{1}{2}\,v_{0,x}^*$, $[A]_{21,19} = \theta_x^* / R_x^2$, $[A]_{21,21} = \tfrac{1}{2}\,u_0^*/R_x^2$,

$[A]_{22,8} = \theta_{x,y}^*$, $[A]_{22,10} = \theta_{y,y}^*$, $[A]_{22,12} = \tfrac{1}{2}\,u_{0,y}^*$, $[A]_{22,14} = \tfrac{1}{2}\,v_{0,y}^*$, $[A]_{22,20} = \theta_y^* / R_y^2$, $[A]_{22,22} = \tfrac{1}{2}\,v_0^*/R_y^2$,

$[A]_{23,7} = \theta_{x,y}^*$, $[A]_{23,8} = \theta_{x,x}^*$, $[A]_{23,9} = \theta_{y,y}^*$, $[A]_{23,10} = \theta_{y,x}^*$, $[A]_{23,11} = u_{0,y}^*$, $[A]_{23,13} = v_{0,y}^*$, $[A]_{23,19} =$

$\theta_y^* / R_x R_y$, $[A]_{23,20} = \theta_x^* / R_x R_y$, $[A]_{23,21} = v_0^* / R_x R_y$, $[A]_{24,11} = 3\theta_x^*$, $[A]_{24,13} = 3\theta_y^*$, $[A]_{24,15} = 2u_0^*$,

$[A]_{24,17} = 2v_0^*$, $[A]_{25,12} = 3\theta_x^*$, $[A]_{25,14} = 3\theta_y^*$, $[A]_{25,16} = 2u_0^*$, $[A]_{25,18} = 2v_0^*$, $[A]_{26,11} = \theta_{x,x}^*$, $[A]_{26,13} =$

$\theta_{y,x}^*$, $[A]_{26,21} = \theta_x^* / R_x^2$, $[A]_{27,12} = \theta_{x,y}^*$, $[A]_{27,14} = \theta_{y,y}^*$, $[A]_{27,22} = \theta_y^* / R_y^2$, $[A]_{28,11} = \theta_{x,y}^*$, $[A]_{28,12} =$

$\theta_{x,x}^*$, $[A]_{28,13} = \theta_{y,y}^*$, $[A]_{28,14} = \theta_{y,x}^*$, $[A]_{28,21} = \theta_y^* / R_x R_y$, $[A]_{28,22} = \theta_x^* / R_x R_y$, $[A]_{29,15} = 3\theta_x^*$,

$[A]_{29,17} = 3\theta_y^*$, $[A]_{30,16} = 3\theta_x^*$, $[A]_{30,18} = 3\theta_y^*$, $[A]_{31,15} = \tfrac{1}{2}\,\theta_{x,x}^*$, $[A]_{31,17} = \tfrac{1}{2}\,\theta_{y,x}^*$, $[A]_{31,23} = \tfrac{1}{2}\,\theta_x^*/R_x^2$,

$[A]_{32,16} = \tfrac{1}{2}\,\theta_{x,y}^*$, $[A]_{32,18} = \tfrac{1}{2}\,\theta_{y,y}^*$, $[A]_{32,24} = \tfrac{1}{2}\,\theta_y^*/R_y^2$, $[A]_{33,15} = \theta_{x,y}^*$, $[A]_{33,17} = \theta_{y,y}^*$, $[A]_{33,23} =$

$$\theta_y^* / R_x R_y. \tag{A4}$$

Individual terms of matrix [G]

$[G]_{1,1} = \partial / \partial x$, $[G]_{1,3} = 1 / R_x$, $[G]_{2,1} = \partial / \partial y$, $[G]_{2,3} = 1 / R_{xy}$, $[G]_{3,2} = \partial / \partial x$, $[G]_{3,3} = 2 / R_{xy}$, $[G]_{4,1} =$

$1 / R_{xy}$, $[G]_{4,2} = \partial / \partial y$, $[G]_{4,3} = 1 / R_{xy}$, $[G]_{5,1} = -1 / R_x$, $[G]_{5,3} = \partial / \partial x$, $[G]_{6,2} = -1 / R_y$, $[G]_{6,3} = \partial / \partial y$,

$[G]_{7,4} = \partial / \partial x$, $[G]_{8,4} = \partial / \partial y$, $[G]_{9,5} = \partial / \partial x$, $[G]_{10,5} = \partial / \partial y$, $[G]_{11,6} = \partial / \partial x$, $[G]_{12,6} = \partial / \partial y$, $[G]_{13,7} =$

$\partial / \partial x$, $[G]_{14,7} = \partial / \partial y$, $[G]_{15,8} = \partial / \partial x$, $[G]_{16,8} = \partial / \partial y$, $[G]_{17,9} = \partial / \partial x$, $[G]_{18,9} = \partial / \partial y$, $[G]_{19,4} = 1$,

$$[G]_{20,5} = 1, \; [G]_{21,6} = 1, \; [G]_{22,7} = 1, \; [G]_{23,8} = 1, \; [G]_{24,9} = 1. \tag{A5}$$